Study of keyhole-porosities in selective laser melting using X-ray computed tomography

Aditi Thanki[1, 2], Louca Goossens[1, 2], Raya Mertens[1, 2], Gabriel Probst[1, 2], Wim Dewulf[1], Ann Witvrouw[1, 2], Shoufeng Yang[1, 2]

[1] KU Leuven, Department of Mechanical Engineering, Celestijnenlaan 300B, 3001 Heverlee, Belgium,

e-mail: aditi.thanki@kuleuven.be, louca.goossens@kuleuven.be, raya.mertens@kuleuven.be, gabriel.probst@kuleuven.be, wim.dewulf@kuleuven.be, ann.witvrouw@kuleuven.be, shoufeng.yang@kuleuven.be

[2] Member Flanders Make, Leuven, Belgium

Abstract

The occurrence of keyhole porosity in selective laser melting (SLM) has so far not been quantified systematically using X-ray computed tomography (X-CT). In this study, keyhole porosity in selective laser molten Ti-6Al-4V grade 23 parts was analyzed using post-process characterizations. Single tracks were produced with optimum, high volumetric energy density and low volumetric energy density parameters on the top of SLM substrate. High volumetric energy density was achieved by either (i) high laser power and optimum scan speed to study the effect of laser power or (ii) optimum laser power and low scan speed to study the effect of scan speed. Keyhole porosity is sensitive to the SLM process parameters. It was observed by using X-CT that a high amount of keyhole porosity was formed below the line scan produced with a high volumetric energy density achieved by optimum laser power and low scan speed; however, a line scan produced with same volumetric energy density but achieved by high laser power and optimum scan speed resulted in less or no voids. The X-CT porosity analysis helped to understand the size, shape, location, and number of keyhole pores that were formed.

Keywords: Selective laser melting (SLM), X-ray computed tomography (X-CT), Keyhole porosity analysis

1 Introduction

1.1 Selective laser melting process

Selective laser melting also known as powder bed fusion is a solid freeform fabrication process where a three-dimensional part is built in a layerwise manner by using a laser to selectively melt metal powder in a powder bed. This was first studied at the end of the'90 [1, 2]. The main advantage of this process is it enables the production of complex metallic parts [3]. In this process, thin layers of powder of the desired material are deposited by means of a powder coating system (fig. 1). These thin powder layers are then molten at selected places by scanning a laser beam over a powder bed according to a predefined scan strategy [4]. Since the material properties of SLM parts are comparable to the properties of the corresponding bulk material [5, 6], applications of the SLM process can be found in many sectors. Examples are the medical sector, e.g. dentistry [7, 8], tool making industries [9, 10, 11, 12], the general manufacturing industry (machine construction, automotive, etc.) and the aerospace industry where the potential of SLM in the production of lightweight structures [13] is investigated.
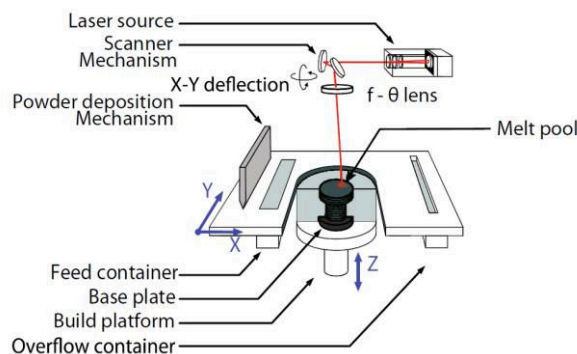

Figure 1. Schematic overview of the SLM process [4].

Current state-of-the-art SLM processes with optimized process parameters normally lead to near 99% part densities. However, local defects or residual porosities can still exist. These porosities can be problematic as they can cause variations in quality and mechanical properties and thus limit the use of SLM parts in particular applications. These unwanted defects might appear due to non-idealities related to the hardware and/or material behavior such as laser acceleration, poor consolidation and material evaporation. The melt pool can be defined as a superheated molten metal bath surrounding the laser-material interaction zone

that traverses with the laser beam. This region is the initiation of the solidified part. Its morphology and thermal distribution are indicators of the final microstructure and part quality [14]. The dynamics of the laser scanner and heat absorption-heat transfer during the process can leads to inhomogeneous melt pool intensity and geometry. There are different mechanisms of pore formation in SLM, one is the keyhole phenomenon [14, 15], but there could be also other reasons for defect formation related to lack of fusion, Rayleigh instability, overheating, melt pool dynamics and external influences.

1.2 X-ray computed tomography
Due to the layer-wise nature of the SLM process, unwanted defects will not always be visible once the part production is complete. In order to investigate the internal part quality, SLM builds are currently examined with post-process characterization techniques, which are either destructive or non-destructive. X-CT is a non-destructive post-process measurement method. X-CT systems consist of three main components: A source, which emits X-rays. A sample, positioned between the source and the detector, which partially absorbs (attenuates) these X-rays (fig. 2). A detector, which captures the remaining of these X-rays, creating a 16-bit grayscale image. Multiple projections (radiographies/images) of the sample are recorded step by step at different rotation angles. Afterwards, when the scanning process has been concluded, a volumetric 3D model of the workpiece is reconstructed through standard reconstruction algorithm [16].
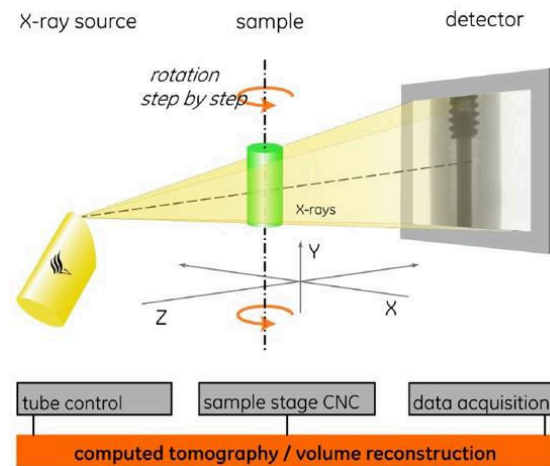

Figure 2. Schematic of setup for the X-ray computed tomography with the flat panel detector [17].

This paper focuses on the research done regarding keyhole porosity formation in SLM builds by using X-CT. After volume reconstruction, X-CT reconstructed volume cross-sections are compared with optical microscopy cross-sections for validation of quantity and location of keyhole pore.

2   Experimental details
SLM parts were built on the in-house developed SLM machine of KU Leuven [18]. This SLM machine is equipped with a fiber laser with a wavelength of 1080 nm and a maximum output power of 1 kW. The focused laser beam has a spot diameter of 50 μm ($\emptyset_{1/e^2}$) on the building plane. Dense SLM substrates (10 x 10 x 5 mm^3) were built first with optimized process parameters from Ti-6Al-4V Grade 23 powder. The powder particle size range was 15 - 45 μm. The SLM substrate layer thickness was 30 μm and the scan strategy was bi-directional with the contour first and with + 90° rotation between consequent layers.

Single tracks were produced subsequently on the SLM substrate with different process parameters (Table. 1). For high volumetric energy density line scans, short lines (6 mm) numbered 1 to 6 (numbering from left to right, see fig. 4) are produced with high laser power and optimum scan speed (condition C1) and long lines (8 mm) numbered 7 to 12 are produced with optimum laser power and low scan speed (condition C2). Same for low volumetric energy density line scans, short lines (6 mm) numbered 1 to 6 are produced with low laser power and optimum scan speed (condition D1) and long lines (8 mm) numbered 7 to 12 are produced with optimum laser power and high scan speed (condition D2) (fig. 3).
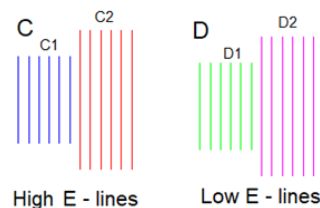

Figure 3. SLM single tracks with different parameters on top of SLM substrate.

X-CT was performed on a Nikon XT H 225 ST machine with a maximum tube potential of 225 kV and multi-material target. Measurement settings were fixed at 180 kV, 12.1 W, exposure time of 2000 ms and 3600 radiographs. Target material for X-rays generation was set to tungsten. Magnification was fixed at a factor of 20, leading to a measurement resolution (voxel size) of 10 µm. Copper filter, for beam hardening reduction, of 1 mm thickness was used. Volume reconstruction was performed using the Feldkamp-Davis-Kress (FDK) algorithm.

2.1 Effect of process parameters

The hypothesized cause of keyhole porosity in SLM parts is that it normally caused by high volumetric energy density [19]. In the current study, high volumetric energy density was achieved either by increasing laser power or by decreasing scan speed. The reason for a different way to produce energy density was to study the effect of laser power and scan speed on keyhole porosity formation. The volumetric energy density was calculated by using the following equation [20]:

$$E = \frac{P}{v\,d\,t}\ J/mm^3$$

Where E is volumetric energy density (J/mm^3), P is laser power (W), v is scan speed (mm/s), t is layer thickness (mm), d is spot diameter (mm).

Table 1. Volumetric energy density values.

Sample ID	Laser Power	Scan Speed	Volumetric energy density (J/mm^3)
Substrate	X	Y	113,33
C1 (lines 1 to 6)	2 * X	Y	226,67
C2 (line 7 to 12)	X	Y / 2	226,67
D1 (lines 1 to 6)	X / 2	Y	56,67
D2 (line 7 to 12)	X	2 * Y	56,67

No lack of fusion was observed using X-CT below line scans produced with low volumetric energy density. This means that these conditions for energy density are still within the optimum process window. It was observed by using X-CT that a high amount of keyhole porosity was formed below the line scans produced with a high volumetric energy density achieved by optimum laser power and low scan speed; however line scans produced with same volumetric energy density but achieved by high laser power and optimum scan speed resulted in no keyhole porosity. In the following chapter, a more detailed analysis of keyhole porosity is given.

3 Keyhole porosity characterization

The X-CT porosity analysis helped to understand the size, shape, location, and number of keyhole pores that were formed. A X-CT scan was performed on the SLM substrate with line scans on top to study the keyhole porosity underneath. (fig. 4) The surface determination (or data segmentation) followed by the volume reconstruction is commonly done via a histogram analysis. It converts voxel data into 3D surface data and determines the interface threshold value (also called isovalue) between the peaks of interest. VGStudio MAX 3.2 software was used for surface determination in this study [21]. It offers two threshold methods: manual and automatic (ISO50 - 50% isovalue). Automatic threshold method (ISO50) is the most employed technique, which considers mid-gray value between the peaks of interest. One of the advantages of the manual threshold method against the automatic is a higher precision of the threshold location. On the contrary, this method is slower and requires longer computation time. Various other methods also exist to identify this threshold [16]: assigning a threshold gray value to ''edge voxels'', interpolating between voxel gray values, searching for maximum gray value derivatives, varying a mid-gray value between air voxel (light) and material voxel (dark) levels, employing a local adaptive gray threshold, etc. In current study, initially automatic thresholding (ISO50) and later manual thresholding was used for the surface determination. By ISO50 thresholding, a total of 136 keyhole pores were found below line scans 7 to 12 (fig. 6).
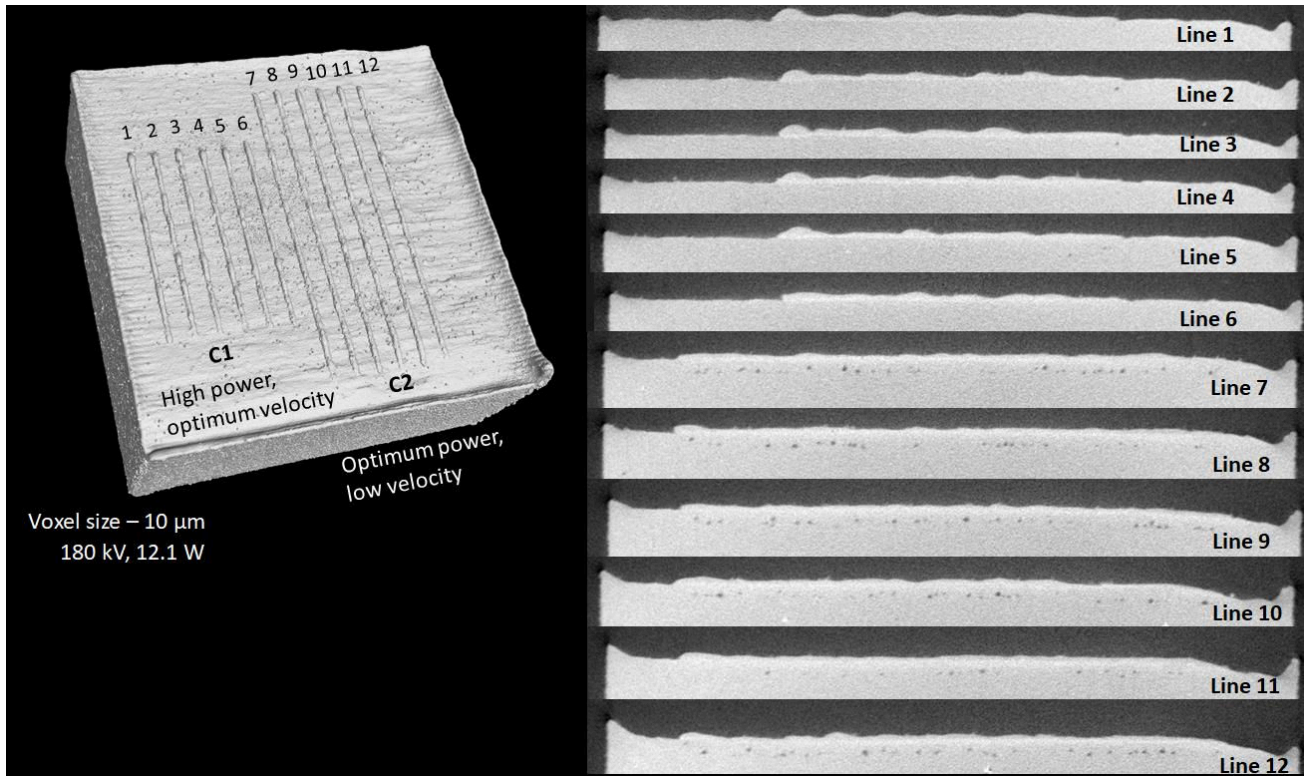
Figure 4. X-CT volume reconstruction of SLM built (left) and X-CT cross-sectional at line scan (right). Lines 1 to 6 (C1) were achieved with high laser power and optimum scan speed and line 7 to 12 (C2) were achieved with optimum laser power and low scan speed.
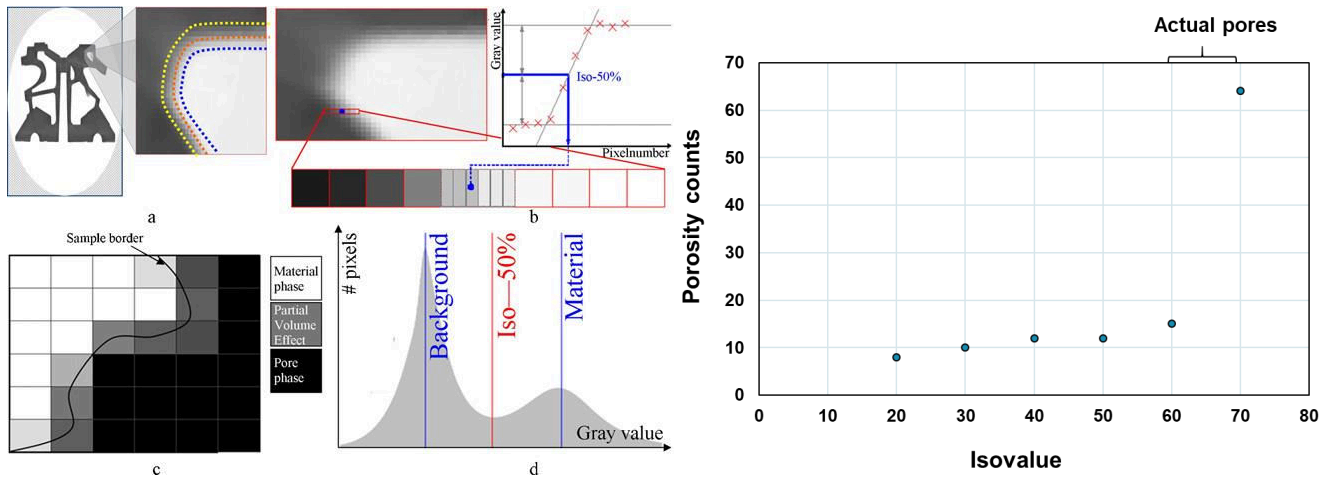

Figure 5. Surface determination & thresholding (left) [17] and iso-value optimization in line 7 for keyhole porosities detection (right).

For manual thresholding, the isovalue was varied from 20 to 70 and the resulting number of pores was compared with a 2D optical microscopy image (fig. 5 right). From optical microscopy, total 23 pores was observed below line 7. According to this result, isovalue should lies in between 60 and 70. The limitation of 2D optical microscopy is that the pore located randomly below line scan can not be observed in single cross-section. Therefore 3D mapping of pore by using 3D optical microscopy is more useful. In the future, once the isovalue has been optimized by using 3D optical microscopy, the same value will be used for the segmentation between air and material.
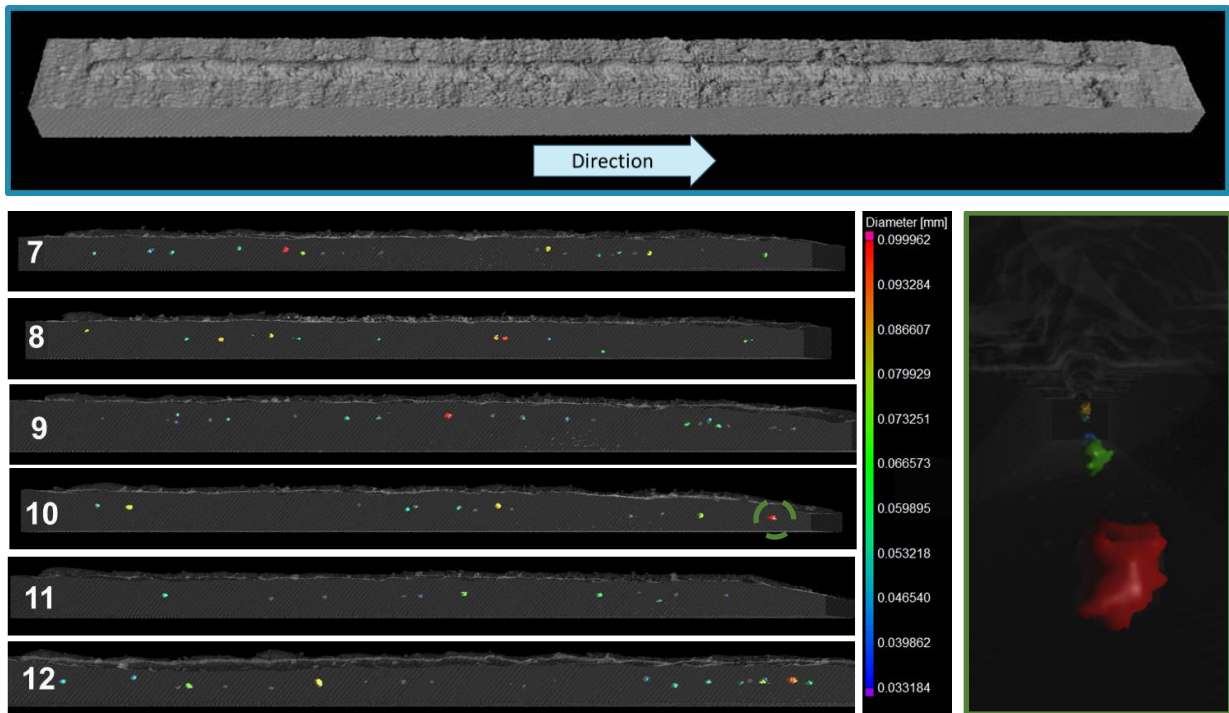
Figure 6. Size (left) of keyhole porosities located below line scan in line 7 to 12 and enlarged shape of keyhole porosity (right) marked in left image in line 10. (Color scale represents diameter range.)
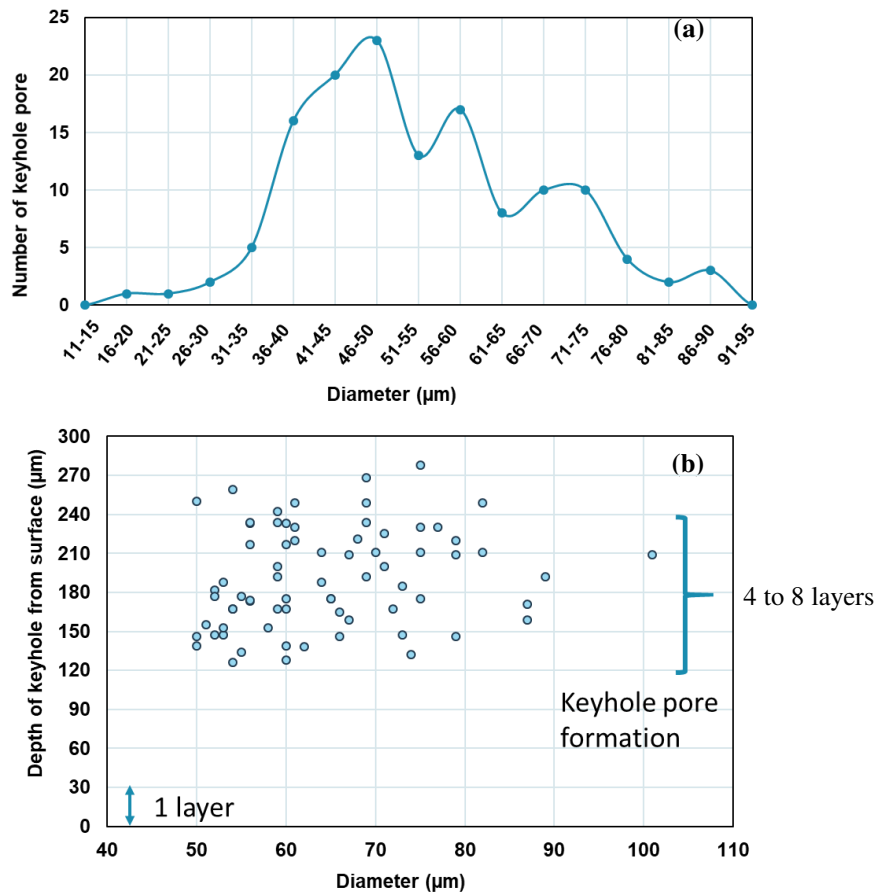

Figure 7. (a) Keyhole pore size distribution below line 7 to 12 (C2) and (b) location of keyhole pores having diameter more than 50 µm from the top surface of the line scan.

Keyhole pore diameter distribution is plotted for line scans 7 to 12 (C2) (fig. 7a). Most of keyhole pore diameter ranges between 35-60 µm. Although the keyhole pores are quite irregular, as can be observed in fig. 6, they were assumed to be spherical for the measurement of their location from X-CT cross-sections (fig. 7b). Keyhole pores with a diameter of more than 50 µm are located 150-270 µm below the top surface of the line scan. This means that these keyhole pores are located 4 to 8 layers below the line scans.

4 Validation of keyhole porosity X-CT analysis with optical microscopy

After the acquisition of the X-CT scans, the obtained results were validated by using optical microscopy. The sample was first ground and then polished with active oxide polishing suspensions (OPS) in order to obtain a cross-section. The etching was performed with Kroll's reagent (6 ml HF, 18 ml HNO$_3$, 300 ml H$_2$O) on the cross-section [22]. This etched cross-section was examined under the optical microscope (fig. 8). One-to-one correlation of keyhole porosity for line 7 from X-CT and optical microscopy cross-section has been first time attempted by comparing the surface topology and the location and size of the pores (fig. 9). Because of the alignment issue of X-CT and optical microscopy cross-sections, not all keyhole pores could be matched.
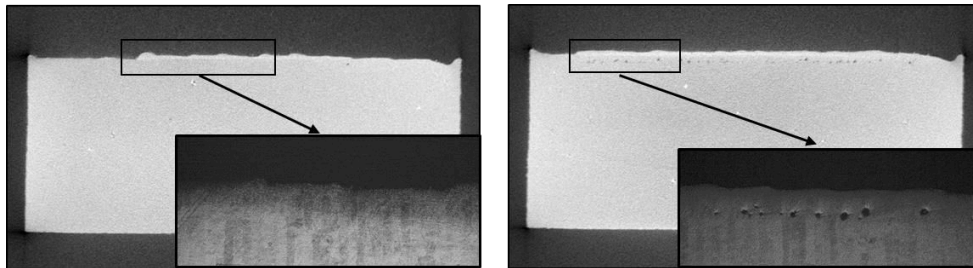

Figure 8. X-CT cross-sectional (background) and optical microscopy images were taken on location showed in the box for line 2 (left) and line 7 (right).
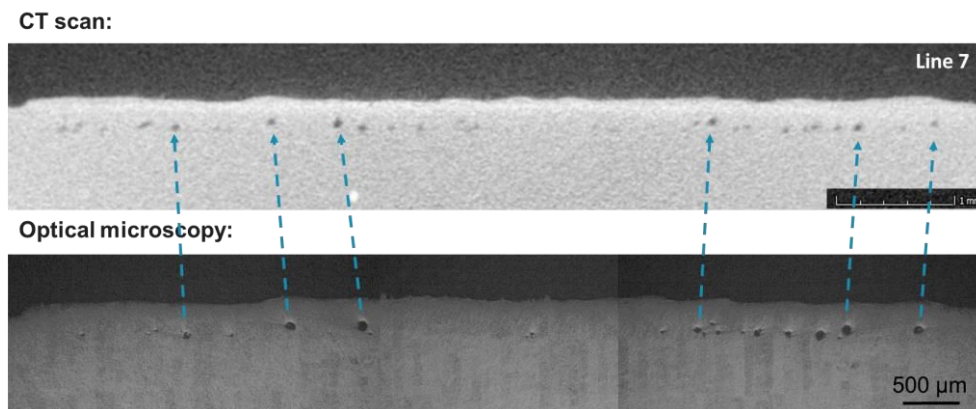

Figure 9. One-to-one correlation of X-CT and optical microscopy cross-sections on line 7.

Conclusions

The qualitative and quantitative study of the effect of process parameters on keyhole pore formation was done. A porosity analysis below SLM single tracks on an SLM substrate was performed by using a Nikon XT H 225 ST X-CT scanner. The results clearly show that keyhole pores were formed at high volumetric energy density achieved with low scan speed and optimum laser power. From X-CT data, the majority of keyhole pore' diameters range from 35-60 µm and the pores having a diameter of more than 50 µm are located 150-270 µm or approx. 4 to 8 layers below the surface of the line scans. The validation of data segmentation of X-CT cross-section was done by comparing it with optical microscopy image of the sample's cross-section. From 2D optical microscopy cross-section, optimum isovalue is confirmed between 60 and 70. The 3D optical microscopy can be used for the optimization of the X-CT isovalue for the surface determination.

In the future, also co-axial optical melt pool monitoring will be used in order to compare the melt pool geometry and intensity to the resulting keyhole porosities. The monitoring signals and the X-ray Computed Tomography data can then be compared for a one-to-one correlation of the in-process and post-process keyhole porosity detection.

Acknowledgments

References

1. Kruth, J., Mercelis, P., Vaerenbergh, J. Van & Craeghs, T. Feedback control of Selective Laser Melting. Proc. 3rd Int. Conf. Adv. Res. Virtual Rapid Prototyp. 1–7 (2007).
2. Wilhelm, M. Direktes selektives laser sintern einkomponentiger metallischer werkstoffe. Diss. Aachen) (1999).
3. Rombouts, M., Kruth, J. P., Froyen, L. & Mercelis, P. Fundamentals of selective laser melting of alloyed steel powders. CIRP Ann. - Manuf. Technol. 55, 187–192 (2006).
4. Kruth, J.-P., Mercelis, P., Vaerenbergh, J., Froyen, L. & Rombouts, M. Binding mechanisms in selective laser sintering and selective laser melting. Rapid Prototyp. J. 11, 26–36 (2004).
5. Thijs, L., Verhaeghe, F., Craeghs, T., Humbeeck, J. Van & Kruth, J. P. A study of the microstructural evolution during selective laser melting of Ti-6Al-4V. Acta Mater. 58, 3303–3312 (2010).
6. Kruth, J.-P., Froyen, L., Kumar, S., Rombouts, M. & Van Vaerenbergh, J. Study of laser-sinterability of iron-based powder mixture. (2004).
7. Kruth, J. P., Van Vaerenbergh, J., Mercelis, P., Lauwers, B. & Naert, I. Dental prostheses by selective laser sintering. 10mes Assises Eur. Prototypage Rapide, Paris 14, (2004).
8. Kruth, J.-P., Vandenbroucke, B., Van Vaerenbergh, J. & Naert, I. Rapid Manufacturing of Dental Prostheses by means of Selective Laser Sintering / Melting. J. Dent. Technol. 24–32 (2007).
9. Abe, F., Osakada, K., Shiomi, M., Uematsu, K. & Matsumoto, M. The manufacturing of hard tools from metallic powders by selective laser melting. J. Mater. Process. Technol. 111, 210–213 (2001).
10. Klocke, F., Wirtz, H. & Meiners, W. Direct manufacturing of metal prototypes and prototype tools. Proc. SFF Symp. 141–148 (1996).
11. Berger, U. & Goebbels, J. Rapid tooling and computer tomography for aluminium casting of automotive components. in uRapid 2001 International users conference on rapid prototyping & rapid tooling & rapid manufacturing (2001).
12. Voet, A., Dehaes, J., Mingneau, J., Kruth, J. P. & Van Vaerenbergh, J. Study of the Wear Behaviour of Conventional and Rapid Tooling Mould Materials. Pmi (2005).
13. Rehme, O. & Emmelmann, C. Rapid manufacturing of lattice structures with selective laser melting. 6107, 61070K (2006).
14. Thompson, S. M., Bian, L., Shamsaei, N. & Yadollahi, A. An overview of Direct Laser Deposition for additive manufacturing; Part I: Transport phenomena, modeling and diagnostics. Addit. Manuf. 8, 36–62 (2015).
15. Shamsaei, N., Yadollahi, A., Bian, L. & Thompson, S. M. An overview of Direct Laser Deposition for additive manufacturing; Part II: Mechanical behavior, process parameter optimization and control. Addit. Manuf. 8, 12–35 (2015).
16. Carmignato, S., Dewulf, W., & Leach, R. (Eds.). Industrial X-ray computed tomography. Springer International Publishing (2018).
17. Kruth, J.P., Bartscher, M., Carmignato, S., Schmitt, R., De Chiffre, L. and Weckenmann, A. Computed tomography for dimensional metrology. CIRP Annals-Manufacturing Technology, 60(2), 821-842 (2011).
18. In-house developed SLM machine of KU Leuven, https://set.kuleuven.be/am/research/machine-design-and-process-optimisation.
19. King, W.E., Barth, H.D., Castillo, V.M., Gallegos, G.F., Gibbs, J.W., Hahn, D.E., Kamath, C. and Rubenchik, A.M. Observation of keyhole-mode laser melting in laser powder-bed fusion additive manufacturing. Journal of Materials Processing Technology, 214(12), 2915-2925 (2014).
20. Ciurana, J., Hernandez, L. and Delgado, J. Energy density analysis on single tracks formed by selective laser melting with CoCrMo powder material. The International Journal of Advanced Manufacturing Technology, 68(5-8), 1103-1110 (2013).
21. VGStudio MAX 3.2 software, https://www.volumegraphics.com/en/products/vgstudio-max.html.
22. ASTM E407-07. Standard practice for microetching metals and alloys (2015).